Research Article

Detection of Papilledema Severity from Color Fundus Images using Transfer Learning Approaches

Merve Kokulu[1], Hanife Göker[2, *]

[1]*Dumlupinar University, Department of Electrical Electronics Engineering, Kütahya, Türkiye*
[2]*Gazi University, Health Services Vocational College, Ankara, Türkiye*

Abstract

Papilledema is edema in the area where the optic nerve meets the eye as a result of increased pressure inside the head. This disease can result in very serious problems, such as abnormal optical changes, decreased visual acuity, and even permanent blindness if left untreated. In this study, an image processing based solution was presented for the detection of papilledema severity from color fundus images using transfer learning approaches. The image dataset includes 295 papilledema images, 295 pseudopapilledema images, and 779 control images. Histogram equalization and the 3D box filter were used for image preprocessing. The images were enhanced with the histogram equalization method and denoised with the 3D box filter method. Then, the performances of EfficentNet-B0, GoogLeNet, MobileNetV2, NASNetMobile, and ResNet-101 transfer learning approaches were compared. The hold-out method was used to calculate the performance of transfer learning. In the experiments, the MobileNetV2 approach had the highest performance with 0.96 overall accuracy and 0.94 Cohen's Kappa. The results of the experiments proved that the combination of the histogram equalization, the 3D box filter, and the MobileNetV2 transfer learning approach can be used for automatic detection of papilledema severity. Compared to other similar studies that are known in the literature, the overall accuracy was higher.

1. Introduction

Pseudopapilledema is a disease in which increased intracranial pressure creates pressure around the optic nerve, affecting vision. In pseudopapilledema, the optic nerve head looks abnormal and swelling. This swelling is not due to increased intracranial pressure or edema in the nerve fiber layer, but papilledema causes swelling of the optic nerve head due to elevated intracranial pressure [1]. The most common causes include optic disc drusen, myelinated nerve fiber and advanced small eye. Symptoms usually affect both eyes simultaneously. Visual blackouts are triggered by a change in position, such as standing up suddenly. Headache is the most common symptom. Other accompanying symptoms include temporary loss of vision, loss of vision due to optical changes, tinnitus and nausea. The risk of papilledema is slightly higher in people with overweight or obesity, obesity, and obese women of childbearing age [2]. The incidence of pseudopapilledema in obese women of childbearing age is 12-20/100,000 person/year compared to 0.5-2/100,000 in the normal population [3]. This disease can result in abnormal optical changes and permanent blindness if left untreated [1]. Patients with pseudopapilledema may face very serious problems if the necessary treatments are not applied. It is a condition that can affect the work life, family life, education life and most importantly the life of the person with this condition.

The most important diagnostic method in pseudopapilledema is careful ophthalmologic examination. Most authors recommend fundus fluorescein angiography (FFA) for the diagnosis of early papilledema [2]. This procedure takes approximately 10 minutes. The yellow medicine given from the forearm veins of the patients reaches the eye vessels in about 12 seconds, during which time the images are recorded with the FFA device. Problematic areas and vessels can be detected in a short time with this method, but since the yellow medicine used during the test is usually excreted in the urine, this test is not performed in patients with known kidney problems. Also, computed tomography (CT) and magnetic resonance imaging (MRI) can be an alternative to ultrasonography in terms of obtaining detailed cross-sectional images to differentiate pathology such as optic disc drusen that may imitate papilledema [2]. Unlike X-rays and CT scans, MRI

---

*Corresponding Author: ▪gokerhanife@gazi.edu.tr 0000-0003-0396-7885

does not carry the risk of ionizing radiation (ionizing radiation harmful to health) [4]. However, it is an expensive examination method due to the high cost of the device, high expenses and expensive contrast medicine [5]. Patients who come with headache complaints and papilledema is detected in neurologic examination may have normal neuroimaging. In this case, cerebrospinal fluid pressure should be measured [3]. Lumbar puncture may be an alternative for this. Lumbar puncture is a diagnostic and/or treatment procedure in which special needles are inserted into the lumbar region of the patient to reach the cerebrospinal fluid. In order to make a definitive diagnosis of certain infectious diseases of the meninges and brain and to reduce intracranial pressure, lumbar puncture is necessary to examine the cerebrospinal fluid [6]. In case a lumbar puncture is not performed, these conditions may not be diagnosed. According to experts, there is currently no other method that can replace lumbar puncture for the diagnosis of these diseases. Problems such as local anesthetic allergy, infection at the puncture site or volume loss (hypovolemia) may occur during lumbar puncture [7].

There are fewer researched studies using transfer learning approaches for the detection of papilledema and pseudopapilledema compared to the diagnosis of other neurological diseases. Gómez-Valverde et al. (2019) obtained an AUC (area under the curve) of 0.94 using VGG-19 architecture for glaucoma detection [8]. Liu et al. (2021) achieved an AUC of 0.99 using ResNet-152 architecture in the detection of optic disc abnormalities [9]. Milea et al. (2020) used the segmentation network U-Net architecture to distinguish optic disc abnormalities from papilledema. They achieved the highest accuracy rate of 91.8% by using DenseNet-121 and DenseNet-201 architectures for classification [10]. Vasseneix et al. (2021) used U-Net for segmentation to detect the severity of papilledema. They achieved 87.9% accuracy rate with VGGNet architecture for classification [11]. Bakır and Yılmaz (2022) used VGG-16, ResNet, InceptionV3 and MobileNet architectures for cataract detection and achieved the highest accuracy rate of 95.51% with ResNet architecture [12]. Ahn et al. (2019) applied Gaussian filtering, normalization and cropping of images to detection of optic neuropathies and pseudopapilledema. They used VGG19, ResNet50, InceptionV3 and their own model. They achieved the highest accuracy of 98.63% in ResNet50 architecture [13]. The development of image processing-based transfer learning models for the diagnosis of pseudopapilledema and papilledema is still an under-researched topic. High performances can be achieved by using image pre-processing and filtering methods in transfer learning approaches. In order to diagnose these conditions easily and with high accuracy, a diagnostic system is needed.

In this study, image preprocessing and filtering were used to achieve high performance. The histogram equalization, an image pre-processing method, was applied to color fundus images. 3D box filter was used as a filtering method. In the study, the effectiveness of transfer learning approaches, namely EfficentNet-B0, GoogLeNet, MobileNetV2, NASNetMobile, ResNet-101 were evaluated. The main contributions of this study are summarized:

a) An image processing based solution was proposed for the detection of papilledema severity from color fundus images using transfer learning, histogram equalization, and 3-D box filtering

b) The performances achieved by the transfer learning approaches were compared to determine the best classification performance.

c) The proposed multi-classification model can help specialists with their busy work schedules and early detection of pseudopapilledema and papilledema.

d) Histogram equalization and filtering methods, which are image pre-processing methods, were applied to the images and high accuracy was achieved in transfer learning approaches.

2. Materials and Methods

2.1. Proposed Model

In this study, an image processing-based solution was proposed to assist in the detection of papilledema severity from color fundus images using transfer learning approaches. The color fundus input images were resized for each transfer learning approach. Histogram equalization was applied to the resulting images. Histogram equalization ensures that the images have the same number of pixels for each brightness level. 3-D box filtering was applied as filtering. It is also known as average filter. Model evaluation metrics of the outputs are calculated and the performances are compared. The flowchart of the proposed model is given in Fig. 1.

2.2. Dataset

Color fundus images were obtained from Kim's Eye Hospital pseudopapilledema data [13]. Fundus images were obtained using a non-mydriatic automatic fundus camera. The dataset includes three labels, namely normal, papilledema, pseudopapilledema. The papilledema group includes 31 retinal diseases, such as posterior uveitis or central retinal vein occlusion, 48 optic neuritis, 17 diabetic optic neuropathy, 177 ischemic optic neuropathy, and 22 papilledema [13].

Normal controls were drawn from routine examinations with no abnormal findings or vision problems. There are 1369 images in total, including 295 papilledema images, 295 pseudopapilledema images, and 779 normal control images. The generated photos had their width scaled to a fixed 500 pixels. Each image was cropped to 240×240 pixels. The dataset of 1369 images is divided into a training dataset of 959 images for model training, and a test dataset of 410 images for model testing.
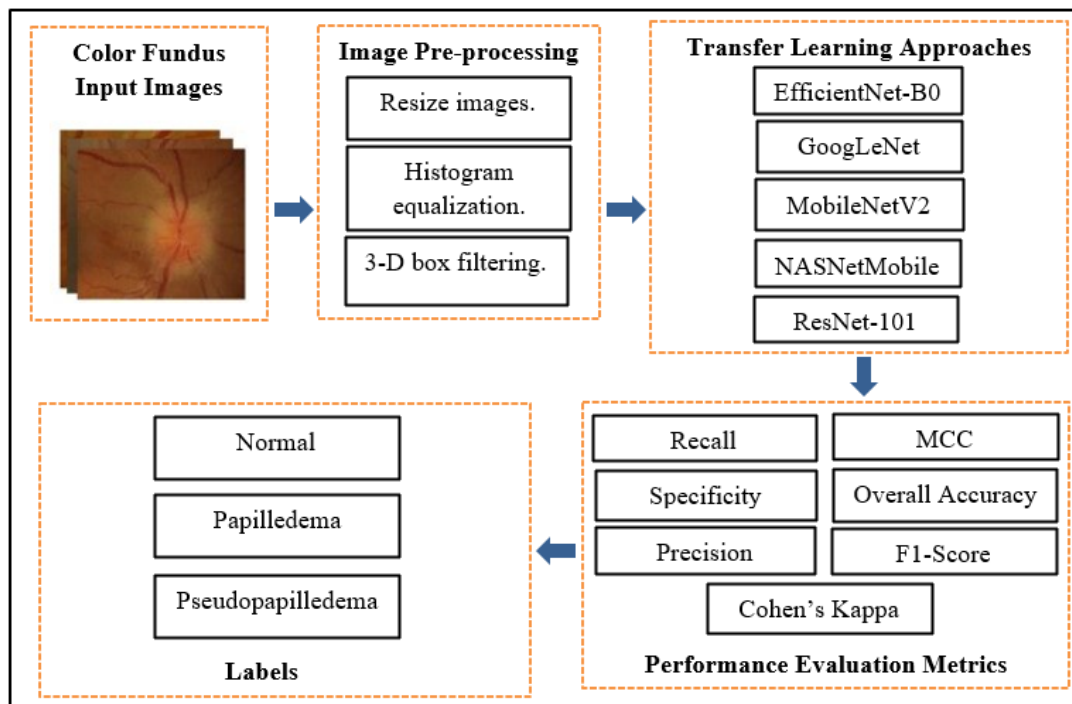
Figure 1. Flow diagram of the proposed transfer learning model.

2.3. Hold-out Method

In this study, the hold-out method was used used to divide the dataset into three. These sets are called "training" and "test" sets. In the training set, the data is trained and the model performs learning. In the test set, the model is tested to see how well the model performs. The hold-out method is useful if a very large dataset is to be processed, if there is a time constraint and there is a very short time for the first presentation of the model. In the dataset, 70% of the images were used for "training set" and 30% for "test set" (see Table 1).

Table 1. Division of data.

	Number of Dataset	**Training Data**	**Test Data**
Normal	779	545	234
Papilledema	295	207	88
Pseudopapilledema	295	207	88
Total	1369	959	410

2.4. Image Pre-processing

Histogram equalization was applied after resizing all images in the dataset. Histogram equalization is one of the most frequently used image enhancement methods. It is a pre-processing method for images whose color values are not uniformly distributed. With this method, it is ensured that there is an equal number of pixels for the brightness levels in the images. The method was developed to remove the color distortion caused by the clustering of color values in a digital image within a certain range of values. After this color distortion is removed, the subtle details in the image become visible. It has a low computation time and can produce very effective results [14].

As an image filtering method, 3-D box filtering was applied. The size of the box filter is specified as a 3-element vector. The size of the box filter was applied to the histogram equalized images as [5 5 3]. 3-D box filtering, performs convolution-based filtering. It is also known as average filter. Average filtering is used to smooth images and is particularly successful in noise reduction applications. This filter works on the principle of replacing each pixel value in the input image with the average value including neighboring pixels [15].

2.5. Transfer Learning Approaches

2.5.1. EfficientNet-B0

The EfficientNet group consists of 8 models from B0 to B7, and the accuracy increases significantly with the model number, but the amount of calculated parameters does not increase. The EfficientNet-B0 architecture uses MBConv, which is an inverted MobileNet with inverted Res bottlenecks. The inverted bottleneck MBConv, formerly known as MobileNetV2, is the fundamental component of EfficientNet [16]. The size of the images has been resized to 224x224 for use in the EfficientNet-B0 architecture. The EfficientNet-B0 architecture is given in Fig. 2.

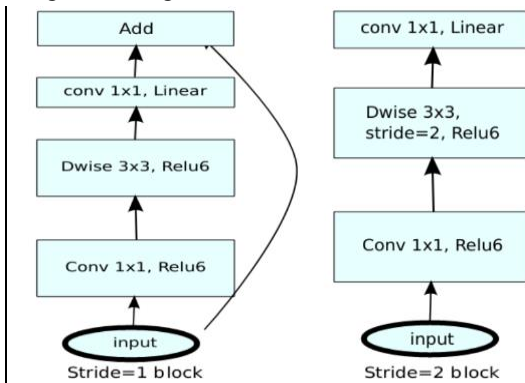
Figure 2. EfficientNet-B0 architecture [17].

Figure 3. MobileNet-V2 architecture [18].

2.5.2. MobileNetV2

The MobileNetV2 is a transfer learning architecture based on an inverted residual structure, with thin bottleneck layers acting as the residual block's input and output. The architecture filters features in the intermediate expansion layer using lightweight and depthwise convolutions. The main difference between MobileNetV2 and the original MobileNet is that MobileNetV2 employs inverted residual blocks with bottlenecking characteristics [18]. The size of the images has been resized to 224x224 for use in the MobileNetV2 architecture. The MobileNetV2 architecture is given in Fig. 3.

2.5.3. ResNet101

The Resnet-101 structure has 101 layers. This design is one of the most advanced ones for ImageNet that is based on the residual neural network learning technique Resnet-101 optimizes the residuals between the desired and the input convolutional features. Desired features are obtained more efficiently and easily when compared to other approaches [19].

In this way, residual optimization can be used to lower the number of factors in a deeper network [20]. The number of layers can be decreased to an effective amount [21] by lowering the number of parameters. The size of the images has been resized to 224x224 for use in the Resnet-101 architecture. The Resnet-101 architecture is given in Fig. 4.
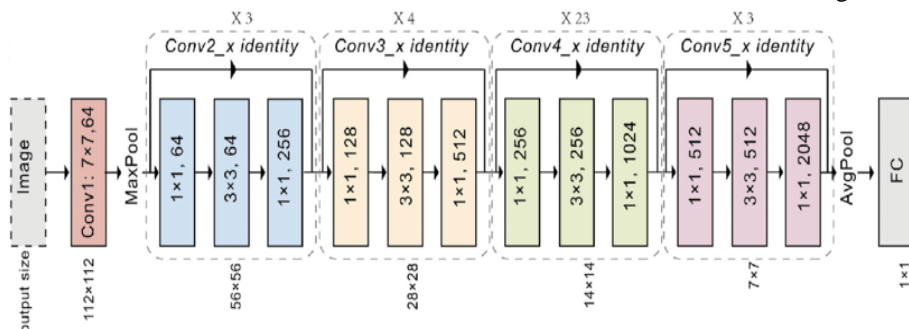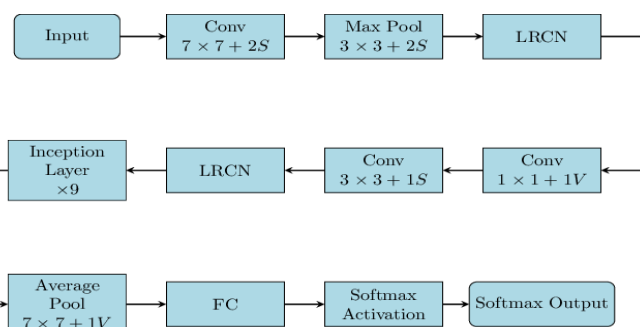

Figure 4. ResNet-101 architecture [22].

Figure 5. GoogLeNet architecture [24].

2.5.4. GoogLeNet

GoogLeNet won the ImageNet 2014 contest with 22 layers and an error rate of 5.7%. In general, it is one of the first CNN architectures to move away from stacking layers of convolution and pooling on top of each other in a sequential architecture. In addition, this new model has a significant impact on memory and power utilization. This is because stacking all layers and adding a large number of filters adds computational and memory costs and increases the probability of memorization. To overcome this, GoogLeNet uses modules connected in parallel [23]. The size of the images was resized to 224x224 for use in the GoogLeNet architecture. The GoogLeNet architecture is given in Fig. 5.

2.5.5. NASNet-Mobile

NASNet networks are scalable ESA architectures and consist of simple blocks such as separable convolution and orthogonalization, which are improved by reinforcement learning [25]. NASNet-based architectures are built by repeating these blocks according to the network capacity [26]. NASNetMobile consists of 12 cells with a capacity of 5.4 million and a multiplication capacity of 564 million [27]. The size of the images was resized to 224x224 for use in the NASNetMobile architecture. The NASNetMobile architecture is given in Fig. 6.
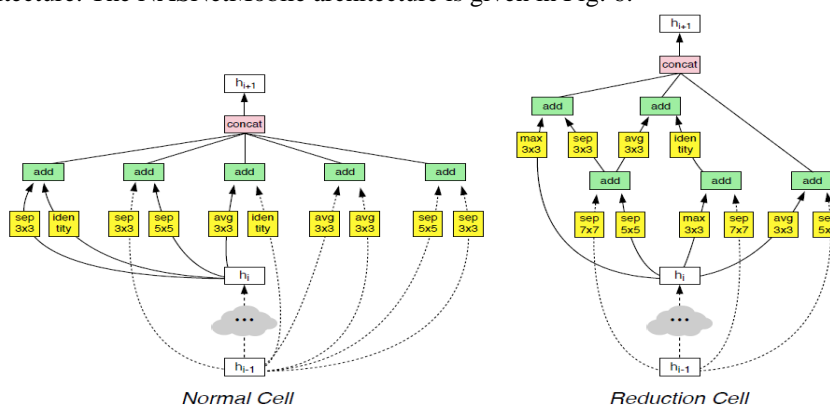

Figure 6. NASNet-Mobile architecture [28].

2.5.6. Performance Evaluation Metrics

The confusion matrix is a tabular form for displaying the prediction model's performance. Each entry in the confusion matrix indicates the number of predictions in which the model classified classes as correct or incorrect. Four parameters are used in the measurements of the matrix: True Positive (TP), True Negative (TN), False Positive (FP), False Negative (FN). The metrics that can be calculated from the confusion matrix obtained in evaluating the performance of the model are given below [29]. Recall, precision, accuracy, f1-score, MCC, specificity, and cohen's kappa statistic are the main performance evaluation metrics [30-31].

$$\text{Overall Accuracy} = \text{Correctly classified values/ Total number of values} \tag{1}$$

$$\text{Recall} = \frac{TP}{TP+FN} \tag{2}$$

$$\text{Precision} = \frac{TP}{TP+FP} \tag{3}$$

$$\text{F1-score} = \frac{2 \times \text{Precision x Recall}}{\text{Precision+Recall}} \tag{4}$$

$$MCC = (TN \times TP) - (FP \times FN)/\sqrt{(TN+FN) \times (FP+TP) \times (TN+FP) \times (FN+TP)} \tag{5}$$

$$\text{Specificity} = \frac{TN}{TN+FP} \tag{6}$$

Kappa statistic, which is frequently used to determine inter-rater reliability. It was developed to determine the degree of agreement between two raters scoring at the classification level. The advantage of the kappa statistic is its easy calculation and practical interpretation. The other and most important advantage is that it is based on correcting for expected agreement by chance [32]. Cohen's Kappa statistic is calculated by following the mathematical formula steps below [33]:

$$P0 = (TP + TN) / (TP + FN + FP + TN)$$

$$Pc1 = (TP+FN) \text{ x } (TP+FP) / [TP+FN+FP+TN]2$$

$$Pc0 = (FP+TN) \text{ x } (FN+TN) / [TP+FN+FP+TN]2 \tag{7}$$

$$Pe = Pc1 + Pc0$$

$$\text{Cohen's Kappa} = (Po - Pe) / (1- Pe)$$

If the kappa statistic is above 0.4, it indicates that the score is not random and is "acceptable fit", a score between 0.6 and 0.8 indicates "significant fit", 0.8 to 1 indicates an almost "perfect fit".

3. Results and Discussions

The dataset used in this study includes images of pseudopapilledema patients, papilledema patients and control participants. Color fundus images were taken from Kim's Eye Hospital pseudopapilledema data [13]. There are 295 pseudopapilledema images, 295 papilledema images and 779 control images. Transfer learning approaches were used to help automatically detect pseudopapilledema and papilledema. The images were resized according to the image input dimensions of the transfer learning approaches. Histogram equalization and 3-D box filtering were applied to the resized images. The hyper parameters used in this study are initial learn rate "0.001", optimizer "sgdm", mini batch size "16", maximum epoch "60", every epoch "shuffle", weight learn rate factor "20" and bias learn rate factor "20". Figure 7 shows the confusion matrices.

EfficientNet-B0		Normal	Papilledema	Pseudo papilledema
TRUE CLASS	Normal	230	1	3
	Papilledema	1	85	2
	Pseudo papilledema	2	5	81
	PREDICTED CLASS			

GoogLeNet		Normal	Papilledema	Pseudo papilledema
TRUE CLASS	Normal	222	5	7
	Papilledema	1	86	1
	Pseudo papilledema	1	2	85
	PREDICTED CLASS			

MobileNetV2		Normal	Papilledema	Pseudo papilledema
TRUE CLASS	Normal	228	1	5
	Papilledema	0	86	2
	Pseudo papilledema	2	3	83
	PREDICTED CLASS			

NASNet-Mobile		Normal	Papilledema	Pseudo papilledema
TRUE CLASS	Normal	225	2	7
	Papilledema	1	86	1
	Pseudo papilledema	5	5	78
	PREDICTED CLASS			

ResNet-101		Normal	Papilledema	Pseudo papilledema
TRUE CLASS	Normal	228	1	5
	Papilledema	0	85	3
	Pseudo papilledema	4	5	79
	PREDICTED CLASS			

Figure 7. Confusion matrices.

Transfer learning approaches were compared in Matlab environment. The same hyper parameter values were used in each transfer learning approach. Confusion matrices were obtained from the transfer learning approaches after the training and testing processes. With the help of the confusion matrix, different metric values can be found and the model accuracy can be evaluated in detail according to the process.

The performance measurement values of the transfer learning approaches derived from the confusion matrix are given in Table 2 and Table 3.

The performance measurement calculated from the confusion matrix are compared with the performance of the transfer learning approaches. The fact that these calculated values are close to 1 indicates that it is a good model. According to Table 2 and Table 3, the transfer learning approach with the highest performance is the MobileNetV2 architecture. The results of the model were found to be 0.99 recall, 0.98 specificity, 0.98 F1- score, 0.97 precision, 0.96 MCC in the normal class; 0.96 recall, 0.98 specificity, 0.98 precision, 0.97 F1-score, 0.95 MCC in the papilledema class; 0.92 recall, 0.97 specificity, 0.94 precision, 0.93 F1-score, 0.91 MCC in the pseudopapilledema class and 0.96 overall accuracy, 0.94 Cohen's Kappa in all classes.

Table 2. Performance metrics values obtained from the confusion matrix of transfer learning approaches.

Model	Outputs	Recall	Specificity	Precision	F1-score	MCC	Overall Accuracy
EfficientNet-B0	Normal	0.99	0.98	0.98	0.99	0.96	
	Papilledema	0.93	0.98	0.97	0.95	0.93	0.9659
	Pseudopapilledema	0.94	0.98	0.92	0.93	0.91	
GoogLeNet	Normal	0.99	0.98	0.95	0.97	0.93	
	Papilledema	0.92	0.97	0.98	0.95	0.93	0.9585
	Pseudopapilledema	0.91	0.97	0.97	0.94	0.92	
MobileNetV2	Normal	0.99	0.98	0.97	0.98	0.96	
	Papilledema	0.96	0.98	0.98	0.97	0.95	0.9683
	Pseudopapilledema	0.92	0.97	0.94	0.93	0.91	
NASNetMobile	Normal	0.97	0.96	0.96	0.97	0.92	
	Papilledema	0.92	0.97	0.98	0.95	0.93	0.9488
	Pseudopapilledema	0.91	0.97	0.89	0.90	0.86	
ResNet-101	Normal	0.98	0.9772	0.97	0.98	0.95	
	Papilledema	0.93	0.9813	0.97	0.95	0.93	0.9561
	Pseudopapilledema	0.91	0.9751	0.90	0.90	0.87	

Table 3. Overall statistics values derived from the confusion matrix of the transfer learning approaches.

Model	Cohen's Kappa
EfficientNet-B0	0.941
GoogLeNet	0.93
MobileNetV2	0.946
NASNetMobile	0.912
ResNet-101	0.925

The accuracy of the transfer learning studies in the literature and the proposed model are given in Table 4. In similar studies using the data sets used in the study, Vasseneix et al, using the VGGNet architecture, achieved 87.9% accuracy [11]. Bakır et al achieved 95.51% accuracy using ResNet architecture [12]. In the proposed model, 96.83% accuracy was achieved on the MobileNetV2 architecture by using methods and architectures different from the image preprocessing/segmentation methods and transfer learning architectures used in other models in the literature.

Table 4. Comparative analysis of related studies.

Researchers	Image Preprocessing/ Segmentation	Dataset	Best Model	Performance
Gómez-Valverde et al. (2019) [8]	Resize images.	2313 images:494 glaucoma-1819 normal.	VGG-19	AUC 0.94
Liu et al. (2021) [9]	Class Activation Mapping (CAM).	Training dataset: 944 images (364 abnormal/580 normal). Testing dataset:151 images (71 abnormal/80 normal), of which 12 images (8 abnormal/4 normal)	ResNet-152	AUC 0.99
Milea et al. (2020) [10]	U-Net	14,341 images:9156 normal disks/2148 papilledema/3037 other abnormalities.	Dense Net	Acc. 99%
Vasseneix et al. (2021) [11]	-	Training dataset:1052 mild-moderate papilledema/1051 severe papilledema Testing dataset:92 mild-moderate papilledema/122 severe papilledema.	VGG Net	Acc. 87.9%
Bakır et al. (2022) [12]	Resize images. Pixel normalization.	1094 color fundus images: 304 left cataract/290 right cataract/ 250 left normal/250 right normal.	ResNet	Acc. 95.51%
Proposed model	Resize images. Histogram equalization. 3-D box filtering.	1369 images: 295 papilledema/ 295 pseudopapilledema/779 normal. Training dataset: 959 images, Test dataset: 410 images.	Mobile NetV2	Acc. 96.83%

4. Conclusions

In this study, a method is proposed to classify pseudopapilledema and papilledema using color fundus images containing 3 different classes. In the proposed method, color fundus images are resized and image pre-processing methods such as histogram equalization and 3-D box filtering are applied. The performances of the pre-processed images are compared in transfer learning approaches. EfficentNet-B0, GoogLeNet, MobileNetV2, NASNetMobile, and ResNet-101 architectures were used as transfer learning approaches. Performance evaluation metrics, namely accuracy, recall, F1-score, precision, specificity, MCC, overall accuracy, and Cohen's Kappa were evaluated. In the study, it was observed that image pre-processing methods and transfer learning approaches provided high performance. The highest performing transfer learning approach was MobileNetV2 architecture with 0.96 overall accuracy and 0.94 Cohen's Kappa. The proposed method can help experts with their busy work schedules and early detection of pseudopapilledema and papilledema. The results of the experiments show that the proposed model is able to achieve the high performance achieved by using the image preprocessing methods and transfer learning approaches used in previous studies with different methods and different transfer learning approaches. This study will help in the automatic detection of pseudopapilledema and papilledema.

References

[1] Öztürk, V. (**2008**). *Papilödem, psödopapilödem, disk ödem ve optik atrofi olgularında optik disk morfolojisinin heidelberg retina tomografisi ile kantitaf değerlendirilmesi*, Yüksek lisans tezi, Başkent Üniversitesi.pp. 1-85.

[2] İbrahimov, E. (**2009**). *Optik disk kabarıklığında retina sinir lifi tabakası kalınlığının OCT ve HRT ile değerlendirilmesi*, Yüksek lisans tezi, Dokuz Eylül Üniversitesi, pp. 1-49.

[3] Şimşek, F., Bilge, N., Ceylan, M. (**2019**). *Erzurum ve çevre illerde psödotümör serebri tanısı ile takip edilen hastaların klinik ve demografik verileri*, Harran Üniversitesi Tıp Fakültesi Dergisi, 16(2), 331-335.

[4] Oyar O., (**2008**). *Magnetik rezonans görüntüleme MRG nin klinik uygulamaları ve endikasyonları*, Harran Üniversitesi Tıp Fakültesi Dergisi, 5(2), 31-40.

[5] Sarıoğlu, B. (**2012**). *Türkiyede MR ve BT görüntüleme işlemlerinin Sosyal Güvenlik Kurumuna ekonomik yükünün değerlendirilmesi*, Yüksek lisans tezi, Başkent Üniversitesi, 1-98.

[6] Çifcibaşı, F. (**2017**). *Acil serviste pediatrik hastalarda lomber ponksiyon yerinin yatak başı ultrason ile belirlenmesinin etkinliği*, Yüksek lisans tezi, Pamukkale Üniversitesi.

[7] Çelik, D. (**2013**). *Çocuklarda lomber ponksiyon iğne derinliğinin tahmin edilmesi*, Yüksek lisans tezi, Selçuk Üniversitesi.

[8] Gómez-Valverde J. J., Antón, A., Fatti, G., Liefers, B., Herranz, A., Santos, A., Sánchez, C.I. & Ledesma-Carbayo, M.J. (**2019**). *Automatic glaucoma classification using color fundus images based on convolutional neural networks and transfer learning*, Biomedical Optics Express, 10(2), 892-913. DOI: 10.1364/BOE.10.000892

[9] Liu, T.Y.A., Wei, J., Zhu, H., Subramanian, P.S., Myung, D., Paul, H.Y., Hui, F.K., Unberath, M., Ting, D.S.W. & Miller, N.R. (**2021**). *Detection of optic disc abnormalities in color fundus photographs using deep learning*, Journal of Neuro-Ophthalmology, 41(3), 368-374. DOI: 10.1097/WNO.0000000000001358

[10] Milea, D., Najjar, R.P., Jiang, Z., Ting, D., Vasseneix, C., Xu, X., Fard, M.A., Fonseca, P., Vanikieti, K., Lagrèze W.A., Morgia, C.L., Cheung, C.Y., Hamann, S., Chiquet, C., Sanda, N., Yang, H., Mejico, L.J., Rougier, M.B., Kho, R., Tran, T.H.C., Singhal, S., Gohier, P., Clermont-Vignal, C., Cheng, C.Y., Jonas, J.B., Yu-Wai-Man, P., Fraser, C. L., Chen, J.J., Ambika, S., Miller, N.R., Liu, Y., Newman, N.J., Wong, T.Y. & Biousse V. (**2020**). *Artificial intelligence to detect papilledema from ocular fundus photographs*, New England Journal of Medicine, 382(18), 1687-1695. DOI: 10.1056/NEJMoa1917130

[11] Vasseneix, C., Najjar, R.P., Xu, X., Tang, Z., Loo, J.L., Singhal, S., Tow, S., Milea, L., Ting, D.S.W., Liu, Y., Wong, T.Y., Newman, N.J., Biousse, V., Milea, D. & BONSAI Group (**2021**). *Accuracy of a deep learning system for classification of papilledema severity on ocular fundus photographs*. Neurology, 97(4), e369-e377. DOI: 10.1212/WNL.0000000000012226

[12] Bakır, H., Yılmaz, Ş. (**2022**). *Using transfer learning technique as a feature extraction phase for diagnosis of cataract disease in the eye*, International Journal of Sivas University of Science and Technology, 1(1), 17-33.

[13] Ahn, J.M., Kim S., Ahn, K.S., Cho, S.H., Kim, U.S. (**2019**). *Accuracy of machine learning for differentiation between optic neuropathies and pseudopapilledema*. BMC Ophthalmology, 19(1), 178. The dataset can be downloaded from: https://osf.io/2w5ce/ DOI: 10.1186/s12886-019-1184-0

[14] Arısoy, M.Ö. & Dikmen, Ü. **(2014)**. *Manyetik belirti haritalarının histogram eşitleme yöntemi kullanılarak iyileştirilmesi*, Yerbilimleri, 35(2), 141-168.

[15] Bozkurt, H. & Çelebi, A.T. **(2021)**. *Ortalama filtre kullanılarak termal görüntülerde sayısal detay iyileştirme*, International Marmara Sciences Congress, Proceedings Book, pp. 103-108.

[16] Tan, M., Le, Q.V. **(2019)**. *EfficientNet: Rethinking model scaling for convolutional neural networks*, 36th Int. Conf. Mach. Learn, ICML 2019, vol. 2019-June, pp. 10691–10700.

[17] Ahmed, T., Sabab, N.H.N. **(2022)**. *Classification and understanding of cloud structures via satellite images with EfficientUNet*, SN Computer Science, 3, 99. DOI: 10.1007/s42979-021-00981-2

[18] Sandler, M., Howard, A., Zhu, M., Zhmoginov, A., Chen, L.C. **(2018)**. *Mobilenetv2: Inverted residuals and linear bottlenecks*, In Proceedings of the IEEE conference on computer vision and pattern recognition (IEEE, USA, 2018), pp. 4510-4520.

[19] He, K., Zhang X., Ren, S., Sun, J. **(2016)**. *Deep residual learning for image recognition*. In Proceedings of the IEEE conference on computer vision and pattern recognition, (IEEE, USA, 2016) pp. 770-778.

[20] Aksoy, B., Salman, O.K.M. **(2022)**. *Prediction of Covid-19 disease with resnet-101 deep learning architecture using computerized tomography images*. Turkish Journal of Nature and Science, 11(2), 36-42. DOI: 10.46810/tdfd.1095624

[21] Chung, Y.M., Hu, C.S., Lawson, A., Smyth, C. **(2021)**. *Toporesnet: A hybrid deep learning architecture and its application to skin lesion classification*, Mathematics, 9(22), 2924. DOI: 10.1109/BigData.2018.8622175.

[22] Tong, Y., Lu, W., Deng, Q.Q., Chen, C., Shen, Y. **(2020).** *Automated identification of retinopathy of prematurity by image-based deep learning*, Eye and Vision, 7, 40. DOI: 10.1186/s40662-020-00206-2

[23] İnik, Ö., Ülker, E. **(2017)**. *Derin öğrenme ve görüntü analizinde kullanılan derin öğrenme modelleri*, Gaziosmanpaşa Bilimsel Araştırma Dergisi, 6(3), 85-104.

[24] Kishore, A., Singh, S. **(2015)**. *Natural language image descriptor*, 2015 IEEE Recent Advances in Intelligent Computational Systems (RAICS) (IEEE, India, 2015), pp. 110-115. DOI: 10.1109/RAICS.2015.7488398

[25] Eryılmaz, F., Karacan, H. **(2021)**. *Akciğer X-Ray görüntülerinden COVID-19 tespitinde hafif ve geleneksel evrişimsel sinir ağ mimarilerinin karşılaştırılması*, Düzce Üniversitesi Bilim ve Teknoloji Dergisi, 9(6), 26-39. DOI: 10.29130/dubited.1011829

[26] Nagrath, P., Jain, R., Madan, A., Arora, R., Kataria, P., Hemanth, J. **(2021)**. *SSDMNV2: A real time DNN-based face mask detection system using single shot multibox detector and MobileNetV2*, Sustainable Cities and Society, 66, 102692. DOI: 10.1016/j.scs.2020.102692

[27] Ba Alawi, A.E., Qasem, A.M. **(2021)**. *Lightweight CNN-based models for masked face recognition*, In 2021 International Congress of Advanced Technology and Engineering (ICOTEN) (IEEE, Yemen, 2021), pp. 1-5. DOI: 10.1109/ICOTEN52080.2021.9493424

[28] Wang, J. **(2020)**. *Anomaly detection of arm X-Ray based on deep learning*, In IOP Conference Series: Earth and Environmental Science, 440(4), 042056. DOI: 10.1088/1755-1315/440/4/042056

[29] Zeng, G. **(2020)**. On the confusion matrix in credit scoring and its analytical properties, Communications in Statistics-Theory and Methods, 49(9), 2080-2093. DOI: 10.1080/03610926.2019.1568485

[30] Çelik, S., & Kasım, Ö. **(2020)**. *Detection of tumor slice in brain magnetic resonance images by feature optimized transfer learning*. Aksaray University Journal of Science and Engineering, 4(2) 187-198. DOI: 10.29002/asujse.820599

[31] Akyol, S., Yıldırım, M. & Alataş, B. **(2023)**. *Multi-feature fusion and improved BO and IGWO metaheuristics based models for automatically diagnosing the sleep disorders from sleep sounds*, Computers in Biology and Medicine, 157, 106768. DOI: 10.1016/j.compbiomed.2023.106768

[32] Bilgen, Ö.B. & Doğan, N. **(2017)**. P*uanlayıcılar arası güvenirlik belirleme tekniklerinin karşılaştırılması*, Journal of Measurement and Evaluation in Education and Psychology, 8(1), 63-78. DOI: 10.21031/epod.294847

[33] Wardhani, N.W.S., Rochayani, M.Y., Iriany, A., Sulistyono, A.D. & Lestantyo, P. **(2019)**. *Cross-validation metrics for evaluating classification performance on imbalanced data*, In 2019 International conference on computer, control, informatics and its applications (IC3INA), IEEE, (pp. 14-18). DOI: 10.1109/IC3INA48034.2019.8949568